IEEE Access
Multidisciplinary | Rapid Review | Open Access Journal

Received October 25, 2021, accepted November 8, 2021, date of publication November 12, 2021,
date of current version November 22, 2021.

Digital Object Identifier 10.1109/ACCESS.2021.3127875

Acoustic Power Transfer Using Self-Focused Transducers for Miniaturized Implantable Neurostimulators

KYUNGMIN KIM[1], (Graduate Student Member, IEEE), SEOK GEUN JANG[2], HAE GYUN LIM[3], HYUNG HAM KIM[1,2,4], (Member, IEEE), AND SUNG-MIN PARK[1,2,4,5], (Senior Member, IEEE)

[1]Department of Convergence IT Engineering, Pohang University of Science and Technology (POSTECH), Pohang 37673, Republic of Korea
[2]Department of Electrical Engineering, Pohang University of Science and Technology (POSTECH), Pohang 37673, Republic of Korea
[3]Department of Biomedical Engineering, Pukyong National University, Busan 48513, Republic of Korea
[4]School of Interdisciplinary Bioscience and Bioengineering, Pohang University of Science and Technology (POSTECH), Pohang 37673, Republic of Korea
[5]Department of Mechanical Engineering, Pohang University of Science and Technology (POSTECH), Pohang 37673, Republic of Korea

Corresponding authors: Sung-Min Park (sungminpark@postech.ac.kr) and Hyung Ham Kim (david.kim@postech.ac.kr)

This work was supported in part by the Basic Science Research Program through the National Research Foundation of Korea (NRF) funded by the Ministry of Education under Grant 2020R1A2C2005385, in part by the Korea Medical Device Development Fund funded by the Korea Government (the Ministry of Science and ICT, the Ministry of Trade, Industry and Energy, the Ministry of Health and Welfare, and the Ministry of Food and Drug Safety) under Grant KMDF PR 20200901 0140-2021-03, and in part by the National Research and Development Program through the National Research Foundation of Korea (NRF) funded by the Ministry of Science and ICT under Grant 2021M3H4A1A03049084.

This work involved human subjects or animals in its research. Approval of all ethical and experimental procedures and protocols was granted by the POSTECH Institutional Animal Care and Use Committee (IACUC) under Application Number POSTECH-2019-0086-R1.

ABSTRACT An emerging neurostimulation therapy utilizes electroceuticals to treat numerous neurological disorders. With the aim to discover novel clinical applications of neural stimulation, device miniaturization has been a key challenge for successful clinical translation of implantable stimulators. The battery size has been a limiting factor in further miniaturization, so wireless power transfer without the use of an implanted battery has gained interest. Among various power transfer techniques, acoustic power transfer (APT) provides substantial benefits for powering implantable devices due to its proven safety and efficiency for human body penetration. In this study, we proposed an APT-based neurostimulator with an integrated self-focused 3.6 MHz acoustic transducer and a receiver circuit composed of a power management module and pulse generator. The size of the entire device was 8 mm × 8 mm × 8.6 mm, which is small enough to be implanted with a small incision. A focused beam generated by an external transmitter was received by another focused beam from a receiver transducer, and this optimized pair of transducers with a receiver circuit generated 1.5 V, 1.3 ms pulse trains, which successfully transmitted stimulation pulses. We adopted a 1-3 composite with a piezolayer to implement a curved aperture, which enabled less-attenuated, focused, and matched beams for maximization of power transfer efficiency. We evaluated APT performance through rigorous bench-top and phantom tests and demonstrated the feasibility of stimulation through an *in vivo* experiment of sciatic nerve stimulation using a rat model.

INDEX TERMS Neurostimulator, miniaturization, implantable device, acoustic power transfer, nerve stimulation.

I. INTRODUCTION

Implantable medical devices (IMDs) have been widely used as diagnostic or therapeutic modalities to treat cardiac rhythm disorders, e.g., arrhythmia, and neurological diseases, e.g., Parkinson's disease. Recently, miniaturization of IMDs, particularly neurostimulators, has become a challenging development aim, as it could lead to the discovery of therapeutic modalities that can treat various neurological disorders more effectively [1], [2]. The greatest hurdle for device

The associate editor coordinating the review of this manuscript and approving it for publication was Alberto Botter.

miniaturization is the size of the battery, which is the main component dominating the allocated space for a neurostimulator. Hence, there is a demand for smaller, alternative biocompatible power sources that could fuel neurostimulators without an implanted battery [3]–[5]. This new powering scheme opened up the possibility for further substantial reduction of device size [6], [7].

Various energy harvesting (EH) and wireless power transfer (WPT) techniques have been proposed as potential batteryless power solutions for implantable devices. EH uses natural physical energies, which are not sufficient or stable in most cases. Compared with EH, WPT is a stable power supply source even for implantable medical devices, since it collects power from outside the body, with adjustable intensity as needed [5], [6]. The electromagnetic (EM) WPT technique, which is currently a representative method of WPT, has been widely accepted for industrial applications, and with its well-known principle and high usability, various near-field to mid-field power transfer methods have been proposed for IMD applications. However, there are remaining challenges, such as short distance [8] and the safety of integrated technology [9] in adapting EM technologies such as RF WPT to IMDs. Using low-frequency RF would increase the lateral size of the antenna [10] and form a direct EM field in the cell [11]. On the other hand, using a high frequency of more than 50 MHz makes the lateral size of the receiver smaller, but energy is attenuated by tissue, which produces a higher specific absorption rate (SAR) [12], [13]. Thus, harmful side effects such as tissue heating are a major concern [14]. With these challenges, potential alternatives to WPT have been investigated.

Acoustic power transfer (APT), which uses the piezoelectric effect to convert acoustic energy into electrical energy, can be alternatives to overcome the above limitations of EM-based WPT techniques [15]–[19]. Although its restriction of air propagation has limited the potential of APT in industrial applications, the human body provides a non-hostile environment for efficient propagation of the acoustic wave. Therefore, in biomedical applications, APT has numerous advantages, such as good transmission efficiency, miniaturization capability, low heat generation, and negligible electrical interference. Besides these introduced advantages, acoustic waves also have advantages for safety that should be considered for implantable devices. Acoustic wave has already been used in various imaging systems and therapeutic applications, so its safety guidelines, international standards, and limitations have been well established [20]–[24]. Although numerous advanced studies toward the development of APT have been reported, there are limitations that must be overcome before it becomes a viable technology [15], [18]. To reduce attenuation by the medium, researchers have used the kHz range of ultrasound. However, a safety concern is that this low-frequency ($<$1.0 MHz) acoustic signal can cause cavitations, which damage tissues. Furthermore, it also increases acoustic beam size, which results in poor spatial resolution [15], [25]. To reduce the beam size and minimize the cavitation effect, it is recommended to use a center frequency above 3.0 MHz, which yields -6 dB lower cutoff frequency above 1.0 MHz. The optimization and beam focusing of acoustic transducers used as a transmitter and receiver for APT are important factors for determining efficiency [26]. While the acoustic lens has been widely used for beam focusing, it can generate a substantial amount of acoustic attenuation. In addition, frequency mismatching between transmitter and receiver transducers can reduce APT efficiency [9]. These issues—operating frequency, attenuation by the lens, and frequency mismatching—have been limiting factors in improving the power efficiency and safety of APT-based IMDs.

In this study, we present a miniaturized APT-based implantable stimulation system composed of an acoustic transmitter transducer, receiver transducer with a power management circuit module, and stimulator circuit. To solve the current limitations of APT, we suggest an operating frequency above 3.0 MHz to minimize the cavitation effect and create a millimeter-wide beam. In addition, we propose a curved aperture enabled by a piezo-composite structure of the transducers to optimize transfer efficiency [27]–[29]. We designed the power management module and pulse generator with a thin profile so that it can fit within a limited space. The designed circuit was implemented using a printed circuit board (PCB) and was combined with the developed APT system to create an APT-based neurostimulator. In the Materials and Methods section, we introduce core strategies and fabrication processes to increase APT performance and describe the design of the neurostimulator circuit in detail. In the Results and Discussion section, we report our findings related to quantitative measurement of the implemented APT system, *in vitro* and *in vivo* experimentation of the APT-based neurostimulator, and analysis of APT performance.

II. MATERIALS AND METHODS

A. IMPLANTABLE NEUROSTIMULATOR

The proposed APT-based neurostimulator is composed of acoustic transducer modules that transmit and receive acoustic energy through the body medium and stimulation circuit module, which includes power management and pulse-generation components. Fig. 1 shows the concept and schematic details of the proposed APT-based neurostimulator. Acoustic power transferred from the external transmitter to the implanted receiver charges the stimulator circuit, which generates and delivers electrical pulses to the sciatic nerve through the wrapped cuff electrode. An electromyogram (EMG) patch was used to monitor muscle twitching as an indicator of successful sciatic nerve stimulation.

We adopted a few customized design and fabrication strategies for transducers to increase transfer efficiency. The core strengths of our approach are the inclusion of a1-3 piezoelectric composite layer, press-focusing, and center-frequency matching for transmitter and receiver

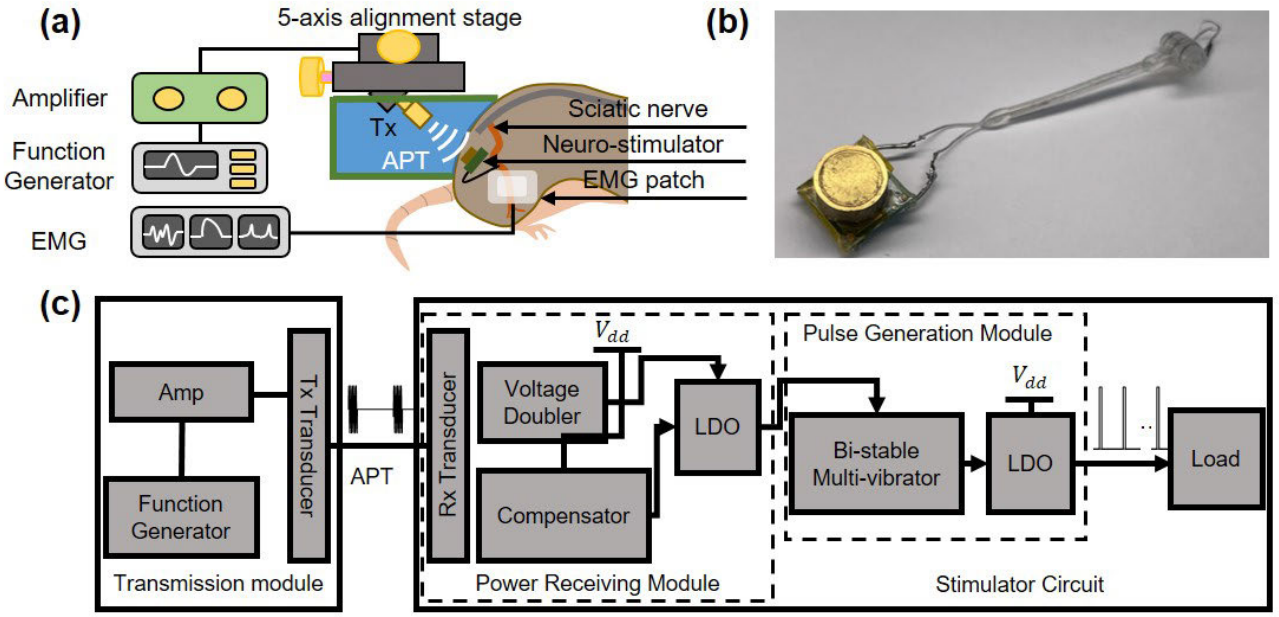

FIGURE 1. Acoustic power transfer (APT) based neurostimulator system, (a) conceptual schematic image of the APT-based neurostimulator system: acoustic power from the transmitter transducer (Tx) is transferred to the receiver transducer of the neurostimulator device; sciatic nerve is stimulated and EMG patch records the EMG signal, (b) photo of a finished prototype of the power receiving module and the stimulator circuit of the APT based neurostimulator system, and (c) the block diagram of the APT based neurostimulator system composed of transmission module, power receiving module and stimulator.

transducers. A piezoelectric composite structure and press-focusing enabled the curved aperture of the transducers, which achieved focused beams without an acoustic lens. Center frequency matching was performed by using identical acoustic stacks with the same thicknesses of constructed layers, which determines the frequency domain characteristics, including center frequency. The power management module supplies energy transferred from the APT module to the pulse generator. The design and fabrication of acoustic transducers are described in section II-B, and details of the circuit module are explained in section II-C.

B. ACOUSTIC TRANSDUCER FOR POWER TRANSFER

Piezoelectric material generates acoustic waves when it is excited by electrical pulses [21]. It also generates electrical pulses when it receives acoustic energy. Acoustic transducer based on the piezoelectric material and optimized by added matching and backing layers is the core component for acoustic power transfer. For better transmit and receive efficiency, the acoustic matching is critical. Double matching layers are used to compensate the difference of acoustic impedances between piezoelectric material and the media. Backing layer is used to reduce the ringing of the acoustic pulse. In addition, the electrode on the top of the matching layer was used to connect with the GND electrode of the transducer, and electrodes on both sides of the piezoelectric material were used for applying the power into the piezoelectric material. The matching layer is conductive and forms the GND connection with the deposited electrode on the piezoelectric material. For optimal efficiency, we recommend two identical transducers for the APT module—one for the transmitter and one for the receiver. The transducers are focused and aligned to match the focal points generated from each other. Focused energy from the transmitter transducer is collected by the receiver transducer at the precise matched focal point; thus, energy loss in the path becomes minimal. The structure of the self-focused transducer is shown in Fig. 2 (a). We selected PMN-PT (PMN-32% PT Type B, CTS Corporation, NJ, USA) for the piezoelectric material, which has a high electromechanical coupling coefficient ($k_t = 0.62$) in the thickness mode of the piezoelectric layer. Of the various piezoelectric composite types, such as 0-3, 2-2, and 1-3, that have been studied, the 1-3 composite structure was selected, as it generates symmetric beams in any plane perpendicular to the beam propagation direction and also achieves press-focusing at elevated temperatures [27]. It is usually produced by patterning the 1-3 composite structure onto piezoelectric material and filling and curing epoxy in the cut-out space [30]–[32]. By adjusting the patterning and material of the composite, we can control the resonance mode and physical parameters such as density, acoustic impedance, dielectric constant, and electrical impedance. In modeling the 1-3 composite with PMN-PT and filling epoxy (Epo-Tek 301, Epoxy Technology, Billerica, MA, USA), we found that the electromechanical coupling coefficient improved from 0.5 to 0.71 at a 70% volume fraction of PMN-PT [28], [29]. The designed center frequency was 3.6 MHz, which yielded a −6 dB frequency passband above 1.0 MHz, thus reducing the risk of

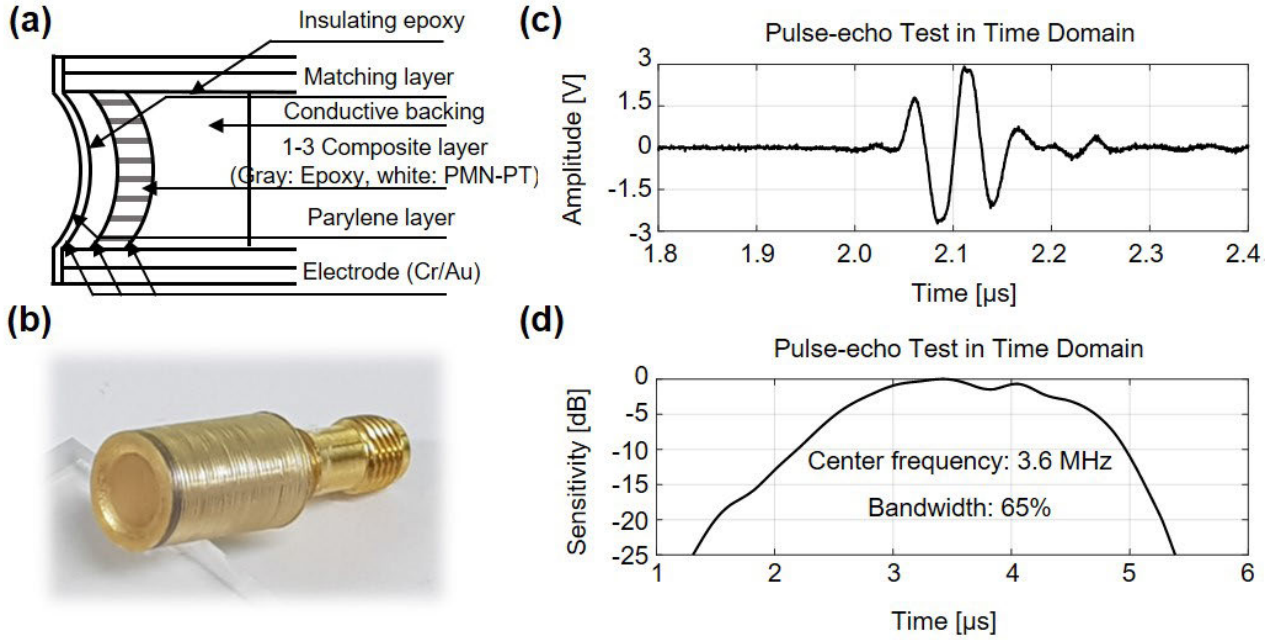

FIGURE 2. Ultrasound transmitter transducer for APT module. (a) Schematic image for structure of transducer, (b) photo of transmitter transducer, (c) time-domain result and (d) frequency-domain result when pulse is applied to the transmitter transducer. Input signal condition: 0 dB gain, 500 Hz PRF, and 50 Ω damping.

cavitation, and generated a millimeter-wide −6 dB lateral beam width [15], [25].

An acoustic lens is generally used to create a focused acoustic beam [33], [34]. However, this additional lens layer caused attenuation of the acoustic wave, and the desired focal strength could not be achieved effectively. Therefore, we adopted the press-focusing technique to focus the beam without a lens by shaping the piezoelectric material layer into a spherically curved surface. However, the press-focusing technique can damage the piezoelectric layer if it is too thick, since the piezoelectric layer cannot be pressed smoothly to form a curved surface. The center frequency of the transducer is inversely proportional to the thickness of the piezoelectric layer, so for 3.6 MHz, as in this case, the piezoelectric layer must be 280 μm, which is too thick to be conformed without causing mechanical failure. We solved this issue by adopting a 1-3 composite structure as shown in Fig. 2(a). The soft epoxy that fills the gap between the pillars of piezoelectric material becomes flexible when heated, which enables the formation of a spherically curved surface when press-focusing is applied.

We built prototype APT transducers by employing a 1-3 composite for the piezolayer and applying the press-focusing technique to form a curved aperture. Its diameter is 6 mm, and it has double matching layers and a backing block, as depicted in Fig. 2(a). To guarantee flexibility, 70% volume fraction of PMN-PT with a >0.7 electromechanical coupling coefficient was selected for the 1-3 composite structure. We deposited Cr/Au (500 Å/1000 Å) electrodes on both sides of the piezoelectric composite layer and bonded the first matching layer of Insulcast 501 epoxy (Insulcast 501, American Safety Technologies, PA, USA) mixed with 2–3 μm silver particles (Silver; Aldrich Chemical Co., MO, USA), which was supported by a backing block (E-Solder 3022, Von Roll Inc, Switzerland). The finished acoustic stack was housed in a brass cylinder and coated with 15 μm-thick Parylene C (SCS, Indianapolis, IN, USA). Fig. 2(b) shows the finished transducer prototype—its pulse-echo characteristics in the time domain (Fig. 2(c)) and frequency domain (Fig. 2(d)) demonstrated −6 dB center frequency (3.6 MHz), and fractional bandwidth (65%). In addition, loop sensitivity can be defined as the ratio of the received signal voltage to the input voltage of the source, calculated as a value in dB. With the result of Fig. 2 and input voltage (123 V_{pp}), we can calculate loop sensitivity (−28 dB at 0 dB gain) [35]. A pulser/receiver (DPR 500, JSR, NY, USA) with 0 dB gain, 500 Hz PRF, and 50 Ω damping was used.

C. NEUROSTIMULATOR POWERED BY APT

Miniaturization of the neurostimulator is essential to reduce the invasiveness of implantable devices. Thus, we implemented a batteryless neurostimulator that requires a power management module that can convert a small AC signal into a large DC signal and supply it to the latter part of the circuit. Additionally, a pulse-generation module is needed to create electrical pulses that are suitable for stimulation following the strength-duration relationship of the nerves. All circuits used in this neurostimulator were implemented by off-the-shelf chips on the PCB for ease of manufacturing.

The power management module consists of a rectifier circuit that rectifies external power and a voltage regulator that outputs a constant voltage for a stable power supply.

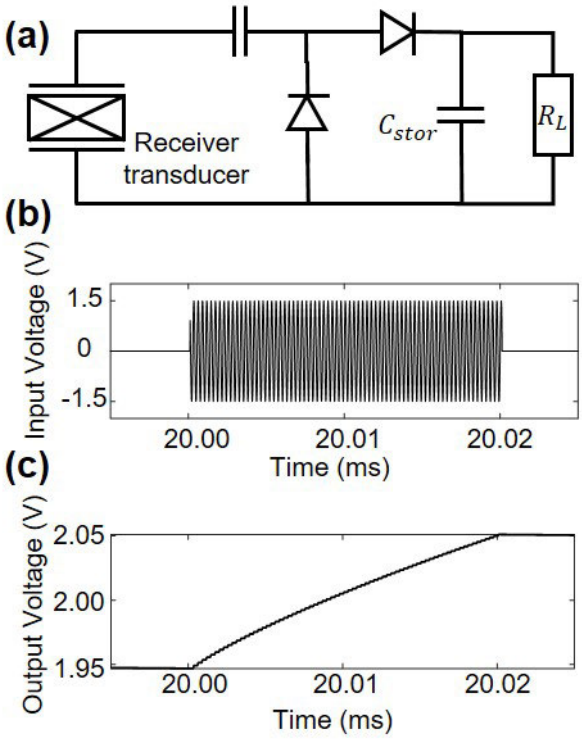

FIGURE 3. (a) Schematic diagram of power receiving module with piezo material as input source and voltage doubler topology. (b) Input signal with $3V_{pp}$, 3.6 MHz sine wave burst, 2 % duty ratio and 1 kHz repetition rate. (c) accumulated voltage at storage capacitor C_{stor} in the power management module.

We designed the rectifier circuit using a network of capacitors and diodes that typically utilize the voltage multiplier principle, switching from low-voltage AC to high-voltage DC electrical power. The rectifier circuit was designed with a reference to half-wave voltage doubler topology (Fig. 3(a)). We simulated the power management circuit by using the SPICE simulation tool (Altium Designer, Altium, CA, USA) to verify the voltage doubler. When the input was a 1.5 V burst signal with a 2% duty ratio of 3.6 MHz sinewave (Fig. 3(b)) and the load impedance was 2.3 kΩ, the storage capacitor voltage in the power management module had a value that rippled between 2.05 V and 1.95 V. This was a charged value, considering the voltage drop of the diode and the power discharged by the load impedance during the off-time of the transducer, as shown in Fig. 3(c). This accumulated energy was transferred to the pulse-generation module at a constant voltage through the low drop-out (LDO) voltage regulator.

The electrical-pulse–generation module consists of an astable multivibrator that receives power from the power management module and an LDO regulator that rectifies multivibrator output and reduces the voltage strength applied to the nerve. The op-amp multivibrator is a kind of oscillator circuit that uses resistors and capacitors to connect the timing network to the inverting input V_- of the op-amp and the voltage-dividing network to the non-inverting input V_+ to generate rectangular waves without digital circuits (Fig. 4(a)).

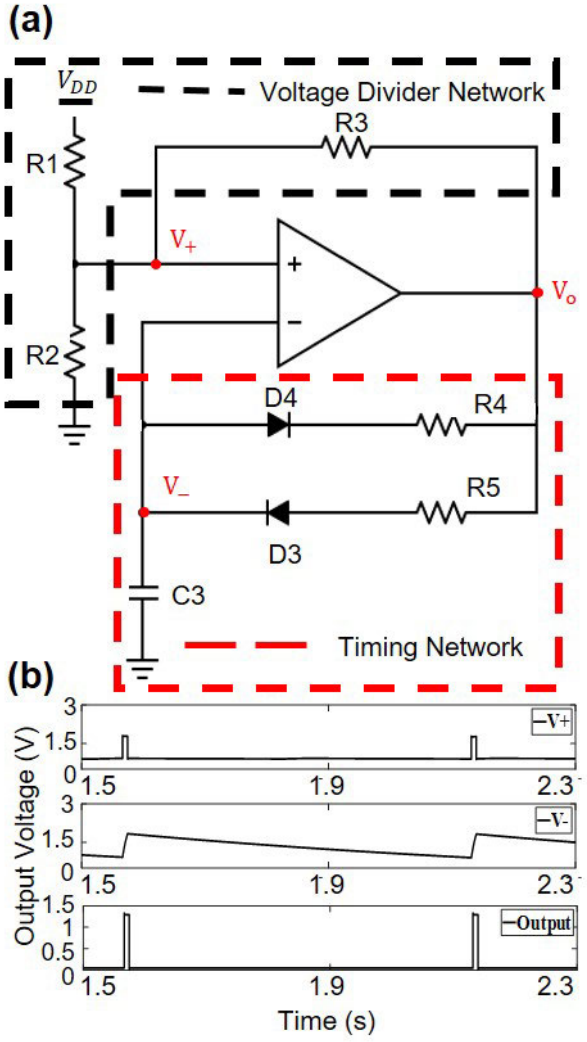

FIGURE 4. (a) Configuration of the astable multi-vibrator, consisting of a voltage divider network at a non-inverting terminal in the op amp and a RC timing network at an inverting terminal. (b) voltage of non-inverting (V+), inverting (V-) and output (Vo) of op amp in the pulse generation module.

The op-amp operates as an analog comparator; one input is used as a reference value, and two outputs are generated depending on whether the reference input is greater or less than the other input value.

$$v_O = V_{dd}(V_+ > V_-) \tag{1}$$
$$v_O = 0(V_+ < V_-) \tag{2}$$

An electric pulse is generated through the charge and discharge of capacitor $C3$. In condition (1), $C3$ is charged. When the voltage of $C3$ is equal to or greater than V_+, such as in condition (2), the charged voltage of $C3$ begins to discharge. The pulse width of the output is determined by the RC time constant components and the feedback ratio according to the reference voltage levels as set by the *R1, R2,* and *R3* voltage divider networks. Equation (3) is derived from Kirchhoff's current law.

$$\frac{V_+}{R2} = \frac{V_{dd} - V_+}{R1} + \frac{v_O - V_+}{R3} \tag{3}$$

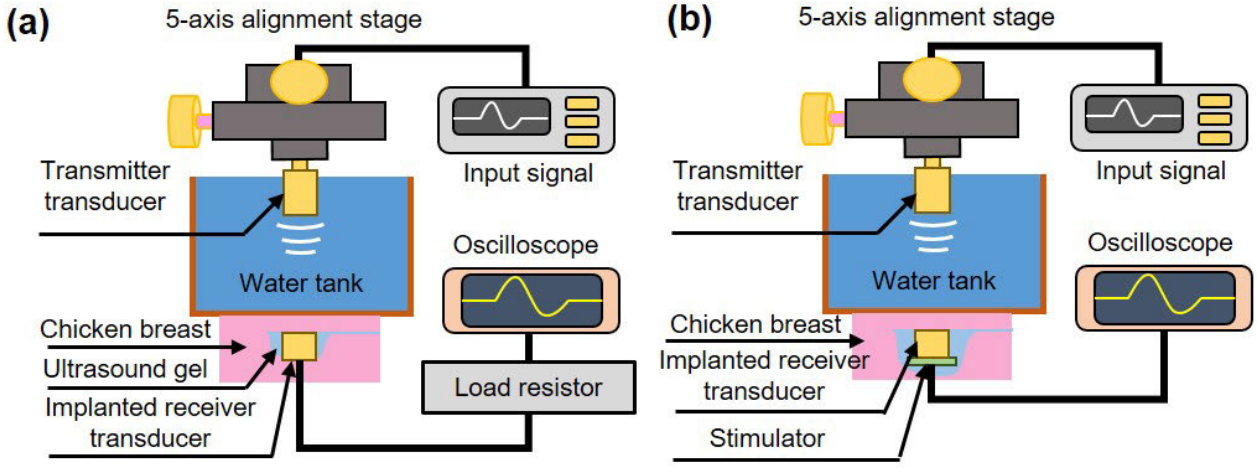

FIGURE 5. Schematic image of in-vitro experiment. (a) To calculate the transmission efficiency of the developed APT system, output signal of receiver transducer was measured by using a load resistor with a constant impedance of 30 Ω. (b) With APT-based neurostimulator, the results were measured at three nodes: the received signal node, the charged capacitor node, and the output signal node. The receiver transducer and APT-based neurostimulator were implanted in chicken breast, and the thickness of the chicken breast was 4.5 mm in the penetration path of acoustic waves. Ultrasound gel was used to prevent the acoustic reflection by trapped air bubble. The bottom of the water tank was made of plastic wrap with very little acoustic attenuation and reflection.

Equation (4) can be derived from equation (3), and the feedback ratio, $\beta_1(V_+ > V_-)$ and β_2 $(V_+ < V_-)$, can be set differently depending on the relation of the resistance values for R1, R2, and R3. For example, when R1 = R2 = R3 = 1 MΩ, β_1 and β_2 become 2/3 and 1/3, respectively.

$$V_+ = \begin{cases} \beta_1 V_{dd} = 2V_{dd}/3 & , V_+ > V_- \\ \beta_2 V_{dd} = V_{dd}/3 & , V_+ < V_- \end{cases} \quad (4)$$

The charging time T_c of $C3$ determines the width of the output pulse and sum of the charging time T_c, whereas the discharging time T_D of $C3$ determines the repeat period of pulses. The equation is as follows:

$$T_c = R5 * C3 \ln(\frac{1-\beta_2}{1-\beta_1}), \quad T_D = R4 * C3 \ln(\frac{\beta_1}{\beta_2}) \quad (5)$$

The operation of this part was also verified by Altium simulation. For $R1 = R2 = R3 = 1$ MΩ, the reference voltage V+ changed to two values: 0.8 V for $\beta_2 * V_{dd}$ and 1.6 V for $\beta_1 * V_{dd}$. As the voltage value of the capacitor $C3$ changes throughout the charging and discharging process, we confirmed that the output pulse was generated by a value comparison between V_+ and V_-(Fig. 4 (b)). By using v_O as the enable pin of the LDO voltage regulator, the pulse parameters are maintained independently of the impedance of the load, and the proper voltage intensity is applied to the nerves. Energy from the power management module is divided into op-amp (max40007ANT+) of the astable multivibrator and low drop-out linear regulator (ADP160ACBZ-1.2-R7).

D. IN VITRO AND IN VIVO EXPERIMENTS

A chicken breast, which has similar acoustic properties to soft tissue such as human muscle, was used as a phantom for the *in vitro* experiment. The experiment setup is depicted in Fig. 5. A transmitter transducer is immersed in the water tank facing downward to generate a transmit beam. The distance between the transmitter transducer and the bottom plane of the water tank was 14.0 mm, and a chicken breast phantom was placed under the water tank. The bottom plane of the water tank was constructed with a plastic wrap that would reveal acoustic reflection of less than 1%, which was an acceptable amount for this experiment. A receiver transducer coupled with ultrasound gel was inserted into the chicken breast phantom, and the thickness of the chicken layer touching the surface of a receiving transducer was set as 4.5 mm. We measured the power transfer efficiency with the connected 30 Ω load resistor, as shown in Fig. 5 (a), and the voltages generated at the stimulator circuit in Fig. 5 (b). Considering that the receiver transducer impedance measured with an impedance analyzer was 33.8 Ω, a 30 Ω load resistor was selected as the optimal load resistor.

The *in vivo* sciatic nerve stimulation experiment utilized an 8-week male SD rat weighing 180–200 g. Rat model experiments were approved by the POSTECH Institutional Animal Care and Use Committee (IACUC, POSTECH-2019-0086-R1). Anesthesia with 2% inhaled isoflurane was administered, and the animal model breathing and temperature were maintained with mechanical ventilation using medical oxygen and a heating pad, respectively. The neurostimulator was inserted into the sciatic nerve after hairs were removed from the skin and a 20 mm vertical incision was made. After inserting the device, a cuff electrode connected to our APT-based neurostimulator was implanted on the sciatic nerve; then, the incision was sutured using a 3–0 Prolene suture.

III. RESULTS AND DISCUSSION

A. TRANSFERRED ACOUSTIC POWER

For the finished self-focused prototype transducers, we measured a series of parameters to characterize the sound field that was generated. We used a membrane-type hydrophone

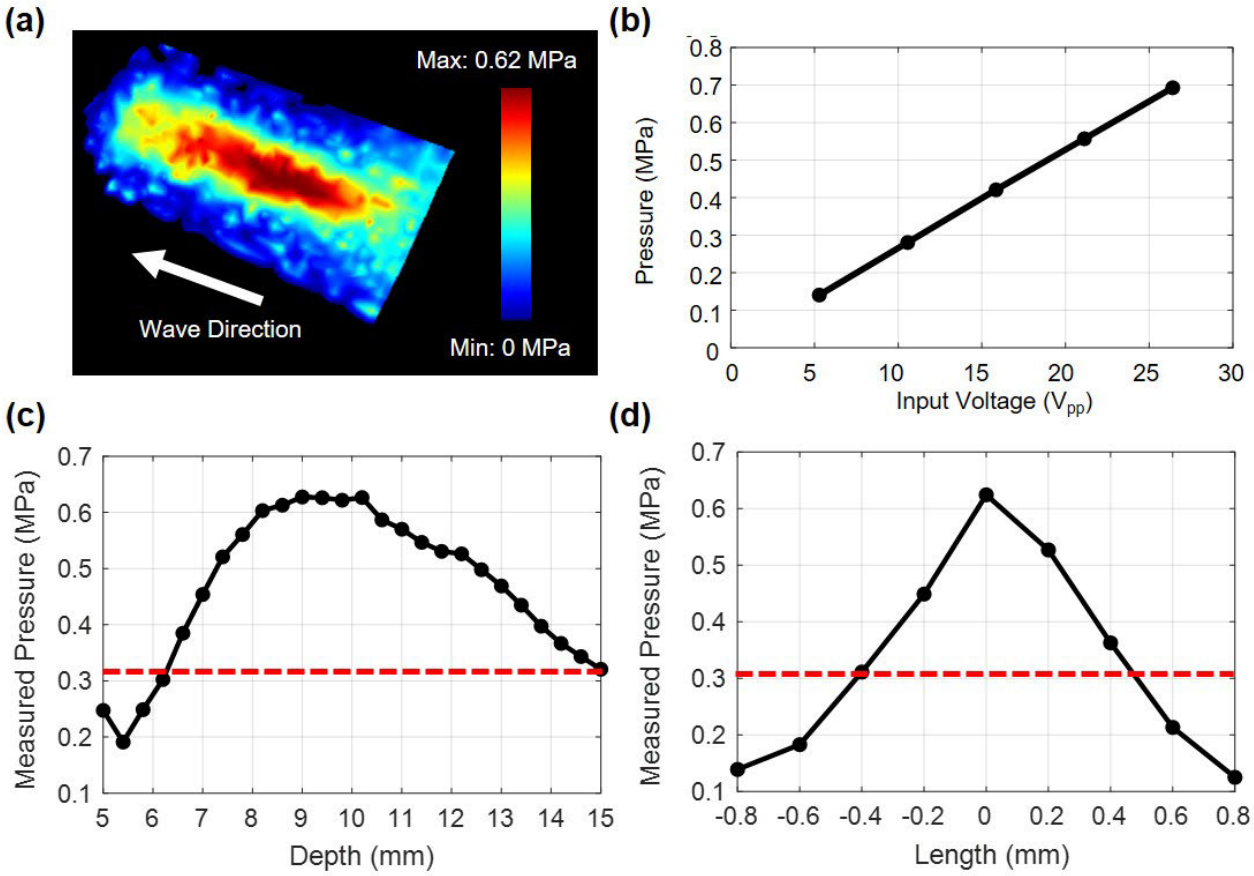

FIGURE 6. The hydrophone measurement results. (a) 3D transmitter beam profile implemented based on hydrophone measurement results. Colorbar: linear-scale [36]. (b) Pressure measurement result of transmitter transducer for input voltage. (c) Measured acoustic beam properties in the axial direction, (d) Measured acoustic beam properties in the lateral direction. Red dotted line means −6 dB.

(D1202, Precision Acoustics Inc., UK) in the water tank to measure the acoustic pressure and intensities at the focal point, and beam profile in the surrounding area. The membrane-type hydrophone used in the experiment has an effective diameter of 0.2 mm, which is suitable for measuring the beam profile having the lateral beamwidth at around 1.0 mm, and after the alignment with the transducer in the water tank, it measures 3D acoustic beam distribution by scanning in the specified 3D volume along the x, y, and z axes. The acoustic pressure map and profiles in Fig. 6 were obtained at a step size of 0.2 mm in the X-Y direction and 0.4 mm in the Z-direction.

The hydrophone experiment conditions were decided as follows: the excitation frequency of the transmit pulse was 3.6 MHz; the input driving voltage ranged from 5.3 Vpp to 26.4 Vpp; the pulse repetition frequency was 1 kHz; and the duty cycle was 1%. The maximum input driving voltage and the duty cycle were set to guarantee safe use of the hydrophone while preventing mechanical failure. The measured voltage data was converted to the pressure map by using the hydrophone sensitivity of 114 mV/MPa at 3.6 MHz, which was rendered in the 3D beam profile as shown in Fig. 6(a). For 3D beam profile rendering, the 3D PHOVIS, a MATLAB-based rendering tool, was used [36]. The pressure was linearly proportional to the input voltage, as shown in Fig. 6(b) ($R^2 = 0.99$). We obtained the axial beam profile (Fig. 6(c)) at the beam axis and the lateral beam profile (Fig. 6(d)) at the focal depth. The axial beam plot shows that the focal point was at 9.0 mm and the −6 dB depth of focus (the width defined by the red dotted line) was approximately 9.0 mm, whereas the lateral beam plot gives a −6 dB beamwidth (as defined by the red dotted line) of approximately 1.0 mm. As a result, the f-number (focal depth/aperture size) was calculated as 1.5, which resulted in a tight focusing pattern that contributed to a more concentrated delivery of power. The density and speed of water used in the hydrophone measurement were 997 kg/cm^3 and 1500 m/s, respectively.

Based on the hydrophone measurement results, we chose the input signal conditions for the *in vitro* and *in vivo* experiments as follows: 3.6 MHz of center frequency, 52.8 Vpp of input driving peak-to-peak voltage, 1 kHz of pulse repetition frequency, and 2% duty cycle. Using the pressure-input voltage relationship based on the linearity in Fig. 6(b), we calculated the acoustic intensities used in *in vitro* and *in vivo* experiments as follows: I_{SPTA} (spatial peak temporal average

intensity) and $I_{SPTA.3}$ (derated I_{SPTA}) were 407 mW/cm^2 and 257 mW/cm^2 respectively [37]–[39]. The measured mechanical index (MI) was 0.73. Thermal index (TI) indicates the thermal effect on the human body caused by the acoustic power. The calculated TI on soft-tissue (TIS) was 0.04, which is far below the recommended TIS of 1.0 set by the U.S. Food and Drug Administration (FDA). Intensity and pressure-related values, $I_{SPTA.3}$, MI, and TIS are lower than the safety limits set by FDA, which are, 720 mW/cm^2 for $I_{SPTA.3}$, 1.9 for MI, and 1.0 for TIS in ultrasound diagnostic imaging equipment [40]–[43].

The measured acoustic data proved that the suggested prototype transducers would be ready for further *in vitro* and *in vivo* experiments. The center frequency of 3.6 MHz satisfied our design goal to reach >3.0 MHz; the lateral resolution of 1.0 mm enabled by the low f-number of 1.5 implemented a sharper beam than that of a high f-number; and the $I_{SPTA.3}$ was well below the FDA limit. Furthermore, It showed an acceptable receiving efficiency, i.e., high enough voltage to run a stimulator circuit; which proves that the system can achieve successful acoustic power transfer that satisfies the safety limit set by the FDA.

B. EXPERIMENTAL RESULTS: IN VITRO

To evaluate the performance of the proposed APT-based neurostimulator, we performed *in vitro* phantom experiments with the setting presented in Fig. 5. We applied the input signal to the transmitter transducer by using the function generator (SG380, SRS Inc, CA, USA) and 50 dB power amplifier (525LA, Electronics & Innovation Ltd, NY, USA). To evaluate APT efficiency, we connected a 30Ω load resistor to the receiving transducer and measured the signal at the load resistor. The *in vitro* experiment conditions were as follows: 3.6 MHz excitation frequency, 5.3–52.8 Vpp input driving voltage, 1 kHz pulse repetition frequency, and 2% duty cycle. The measured results at the load resistor are summarized in Fig. 7. We measured the impedance of the transmitter transducer, 39.3 Ω, with an impedance analyzer (E4990A, Keysight Inc., CA, USA). At 52.8 Vpp input driving voltage, we obtained 354.84 mW input power into the transmitter transducer, and 9.43 mW output power from the receiver transducer. Thus, the power transfer efficiency of the APT system was 2.7 %.

The APT-based neurostimulator was fabricated by electrically connecting the conductive backing layer of the receiver transducer and the input node of the neurostimulator circuit by using a conductive epoxy. We measured the signals at the receiver signal node, charged capacitor node, and output signal node using an oscilloscope (DPO 3032, Tektronix Inc, OR, USA) and measuring probe (P6139B, Tektronix Inc., OR, USA). The measurement results are shown in Fig. 8. The receiver transducer acquired 3 V_{pp} pulses (Fig. 8(a)), which was generated from the transmitter transducer and attenuated in water and chicken breast. This 3.6 MHz tone burst signal with 2% duty ratio and 1 kHz PRF were supplied to the input node of the neurostimulator circuit. As shown

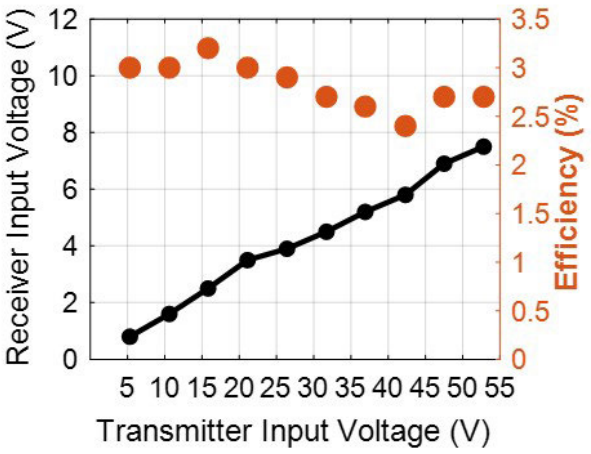

FIGURE 7. Receiver output voltage and efficiency results graph for the transmitter input voltage. We confirmed that the power transmission efficiency of APT system was 2.7% in the in vivo condition at 52.8 V_{pp} input voltage.

in Fig. 8(b), despite the fast consumption rate due to the low input impedance of the voltage regulator used in the stimulator circuit, the storage capacitor in the power management module was charged to a voltage that could drive the entire circuit. The measured voltage shown in Fig. 8(b) was 0.2 V lower than the simulation result shown in Fig. 3(c), because the forward voltage drop of the diode was affected by parameters such as the varying temperature and current in the APT source that occurred during the experiment; however, the simulation error was still within the acceptable range. The charging and discharging time of the capacitor C3 connected to the inverting terminal of the op amp in the pulse-generation module were measured as Fig. 8(c). Fig. 8(d) shows that the output pulses occurred with a 1.7 Hz repetition rate. The output pulses were synchronized with the charging and discharging timing of the capacitors in the pulse-generation module (Fig. 8(c), (d), and (e)), which verified the operation of the stimulator. The result shows that the neurostimulator can create electrical pulses with an appropriate pulse width and sufficient intensity that satisfies the strength-duration curve for nerve stimulation [44]. In contrast to the EM supplying continuous energy, APT can conserve energy during transfer in a discontinuous way, but there may be voltage discharge at the power management module during the off-time. Therefore, the stimulator was designed to compensate for the fact that natural discharge occurred during the off-time.

The previous studies, which use a reasonable size for implantable devices and frequencies above 1 MHz to ensure safety, are listed in TABLE 1. It shows that the APT efficiency using frequencies above 1 MHz was approximately 0.002% to 2.11% [45]–[48]. Because APT efficiency depends on various parameters, such as frequency, medium, distance between transmitter and receiver, aperture of transducers, system load impedance, etc., it is difficult to compare those reported results directly. However, our suggested approach has clear

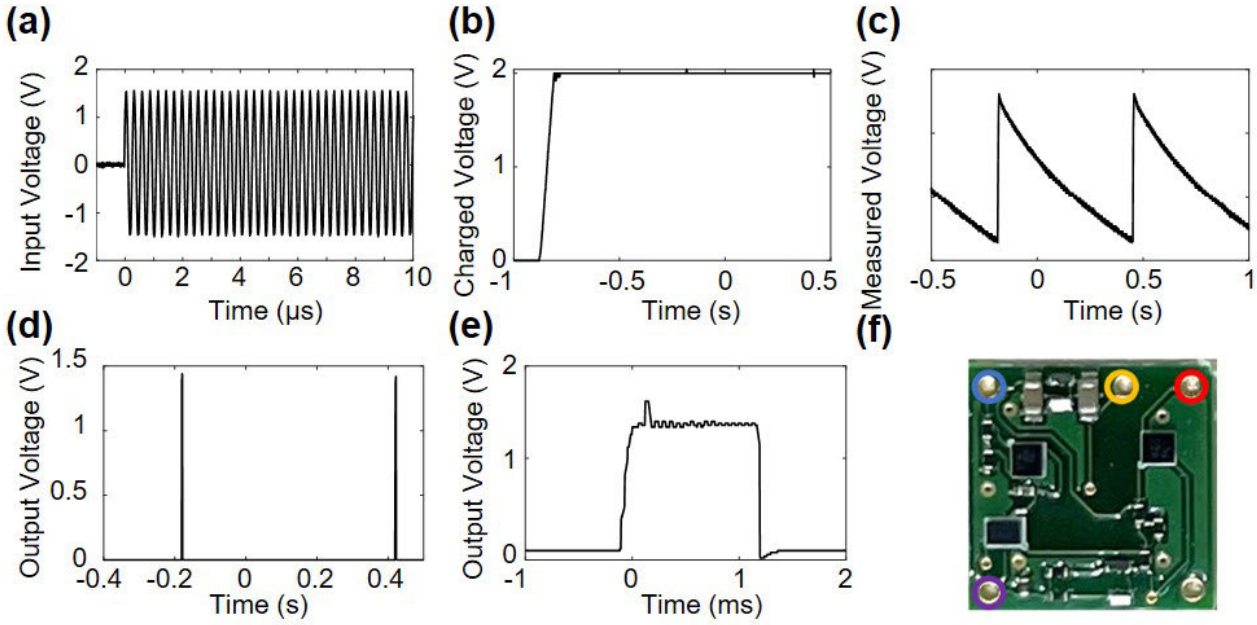

FIGURE 8. Measured voltage at each node of implantable neurostimulation circuit; (a) input burst signal from receiving transducer; (b) voltage stored at storage capacitor of power management module; (c) voltage at inverting input of the op amp; (d) electrical pulses with 1.7 Hz repetition rate at output node of neurostimulator circuit; (e) zoomed output pulse wave form; (f) implementation of neurostimulator by PCB with input: yellow hole, storage capacitor: blue hole, inverting input of the op amp: purple hole, output of the stimulator circuit: red hole.

TABLE 1. Comparison for parameters and performance in the studied APT systems.

Group	Tx Diameter	Input Power	Receiver Diameter	Output Power	Frequency	Depth	Medium	Efficiency
Unit	mm	mW	mm	mW	MHz	cm	-	%
Meng et al. [40]	10.8	-	1.2	-	1.8	3	Castor oil	2.11
Chang et al. [41]	20	-	0.6	-	1	6	Castor oil	1.93
Seo et al. [42]	6.35	29.2 ($\mu W/cm^2$)	0.127 x 0.127	20.64 (pW)	5	3	Water	0.002
Song et al. [43]	20	-	1 x 5	2.48	2.3	20	Water	0.4
Song et al. [43]	30	-	2 x 2	8.7	1.15	20	Water	1.7
This work	6	354.84	6	9.43	3.6	1.85	Chicken breast & water	2.66

advantages over previous reports. First of all, we used the tissue-mimicking chicken breast phantom to test a condition that is similar to a real-world condition. Although we used a relatively high frequency, 3.6 MHz for APT, our system emitted 9.43 mW of high output power. The depth of the receiver circuit, 1.85 cm, is a reasonable choice considering the operating frequency of 3.6 MHz. The size of the transmitter transducer that satisfied all of the parameters was also the smallest. The efficiency of 2.7 % was a definite improvement compared to that reported in other APT studies that used an operating frequency higher than 1.0 MHz. Over all, our method of employing two focused, matched ultrasound beams with a curved aperture may be a promising route for further improvement of APT.

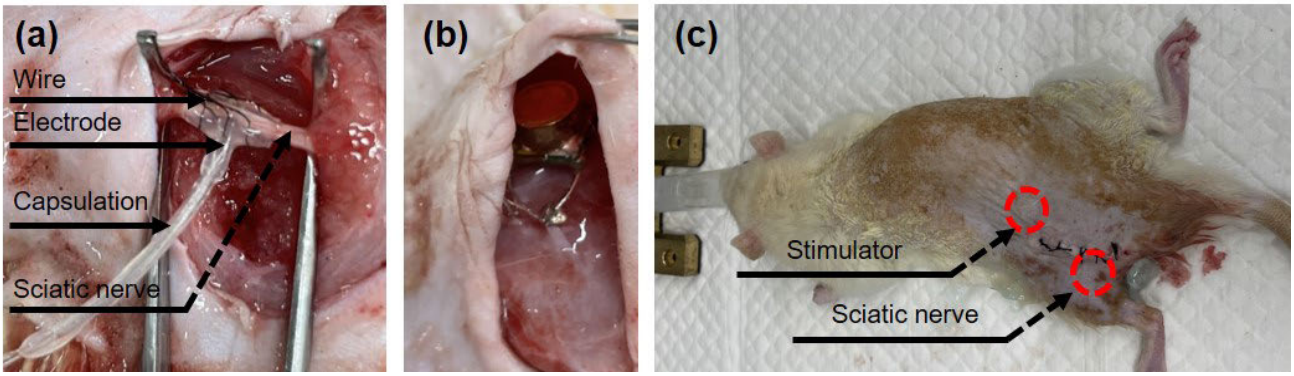

FIGURE 9. Images of sciatic nerve stimulation experiment. (a) The cuff-electrode was connected to the sciatic nerve by the wire-binding. The electrode was protected by a capsulation tube fabricated with a biocompatible material, and it transmitted the simulation signal generated by the neurostimulator to the sciatic nerve. (b) The Expanded image for implanted neurostimulator in the body of the rat. Since the tissue of rat is not ideal, it cannot be parallel to the tissue, the transmitter and receiver transducer. This problem can cause deflection of the acoustic beam and interfere with the alignment of the APT system. In order to align the APT system, we anesthetized the rat and manually used a 5-axis motor stage installed in the transmitter part in this experiment. (c) Full image of a rat implanted with neurostimulator.

C. EXPERIMENTAL RESULTS: IN VIVO

Finally, an *in vivo* experiment was performed using the rat model to confirm whether the proposed system could effectively induce nerve stimulation. The sciatic nerve runs along the hip joint and down the lower limb, thus causing the legs to shake when the electrical pulse successfully stimulated the nerve. Therefore, we aimed to stimulate the sciatic nerve and monitor leg muscle twitching by using electromyography (EMG). To apply stimulation signals to the sciatic nerve, we connected cuff electrodes (microcuffs, MicroProbes, MD, USA) to the output node of the APT-based neurostimulator. As shown in Fig. 9, the electrodes were connected to the rat's sciatic nerve, and the entire APT-based neurostimulator was implanted in the rat.

The same input signal conditions as used for the *in vitro* experiment were applied. EMG signals were recorded with three electrodes (+ at the sole of the foot, − at hind limb, GND at the back) while stimulating the sciatic nerve using a monophasic electrical waveform with a 1.3 ms single pulse. Rat EMG data were recorded by the data acquisition system (MP160 EMG100, BIOPAC System, Inc, CA, USA), and the data were analyzed by analysis software (AcqKnowledge, BIOPAC System, Inc, CA, USA). An EMG signal spike occurred immediately after the stimulation. Because the electrode was attached to the sole of the rat, the leg muscles trembled and the foot shook up and down, which was interpreted as having the same waveform as that depicted in Fig. 10. By confirming that the leg vibrated when the sciatic nerve was stimulated, we proved that the implemented APT-based neurostimulator successfully stimulated the nerves.

Misalignment of the transmitter and receiver transducers can reduce transmission efficiency and cause safety problems of delivering power to an unintended area. Movement generated by stimulation of the sciatic nerve, such as heartbeat, could be attributed to changes in the position of the device, which may cause slight misalignment between transducers.

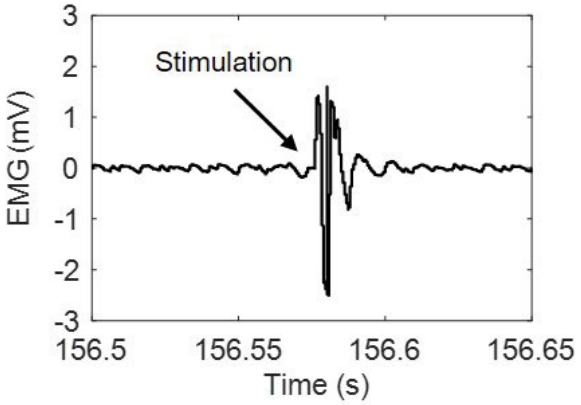

FIGURE 10. The measured EMG signal of rat due to the muscle twitch when the energy transferred from the outside is sufficiently charged to activate the APT-based neurostimulator.

Since the proposed single-element transducer has a fixed focal point, we should adjust the position of the transducers to re-match them if the beams are misaligned. The array transducer with multi-elements is a potential solution since it can form and steer the beam at different depths and in different directions. This will not only solve the misalignment problem but also further enhance the efficiency [49], [50]. A micro-scale two-dimensional (2D) array transducer using bulk piezoelectric material is under development [51], [52]. Although performance is insufficient, 2D array transducer fabricated with microelectromechanical systems (MEMS) technology have been the focus of several studies [43]–[55]. One-dimensional (1D) and 2D array transducers will be key components for a fully optimized APT system.

Finally, the *in vivo* experiment results confirm that our proposed APT based system can stimulate the sciatic nerve of the rat. We focused on muscle twitching by stimulating the sciatic nerve with a 1.5 V 1.3 ms-long signal with a low repetition rate of 1.7 Hz. It should be emphasized that we were able to generate the pulse train with intensity and

pressure levels that were much lower than the safety limit set by the FDA for diagnostic ultrasound imaging systems. More importantly, the proposed APT neurostimulator can be easily modified to generate different types of stimulation pulses for different applications since the proposed system is composed of off-the-shelf commercial ICs; thus, the design can be altered to form different shape pulses. Other applications include but are not limited to peripheral nerve stimulation for regeneration after crush injury [56], vagus nerve stimulation for treating hypertension [57], and tibial nerve stimulation for treating the overactive bladder [58], [59]. Our study proves the feasibility of APT for implantable neurostimulators. By tuning the acoustic parameter and modifying the receiver circuit design, we can control the delivered power level and magnitude, as well as the frequency and width of the stimulation pulses. We expect a variety of implementations that are customized for each individual stimulation need.

IV. CONCLUSION

Herein, we proposed an APT-based batteryless neurostimulator with improved efficiency achieved via self-focused transducers and customized receiver circuits. We optimized the transducers used in the APT system by selecting 3.6 MHz as the operating frequency to reduce cavitation risk, reduced attenuation by using a curved aperture, and matched the focused transmission and receiver beams. We fabricated the receiver circuit module using a low-cost PCB and proved that the entire system runs without a battery. Through *in vitro* and *in vivo* experiments, we demonstrated that the proposed system could deliver power from an external ultrasound source to stimulate the sciatic nerve of the rat successfully.

The advantages of APT, such higher power due to focused beams and its compact form within an implanted circuit, which is achieved by using batteryless technology, will stimulate ongoing investigation in this research area. Current challenges in beam alignment and integration with an external power source should be addressed. Increasing demand for more compact IMDs will lead to new innovations, and optimization of the APT system will function as a key component.

ACKNOWLEDGMENT

(Kyungmin Kim and Seok Geun Jang contributed equally to this work.)

REFERENCES

[1] C. C. Horn, J. L. Ardell, and L. E. Fisher, "Electroceutical targeting of the autonomic nervous system," *Physiology*, vol. 34, no. 2, pp. 150–162, Mar. 2019.

[2] P. Sokal, M. Harat, P. Zieliński, and S. Kierońska, "Tibial nerve stimulation with a miniature, wireless stimulator in chronic peripheral neuropathic pain," *J. Pain Res.*, vol. 10, p. 613, Mar. 2017.

[3] S. Mishra, "Electroceuticals in medicine—The brave new future," *Indian Heart J.*, vol. 69, no. 5, pp. 685–686, Sep. 2017.

[4] B. I. Rapoport, L. Turicchia, W. Wattanapanitch, T. J. Davidson, and R. Sarpeshkar, "Efficient universal computing architectures for decoding neural activity," *PLoS ONE*, vol. 7, no. 9, Sep. 2012, Art. no. e42492.

[5] Z. L. Wang and W. Wu, "Nanotechnology-enabled energy harvesting for self-powered micro-/nanosystems," *Angew. Chem. Int. Ed.*, vol. 51, no. 47, pp. 11700–11721, 2012.

[6] B. Shi, Z. Li, and Y. Fan, "Implantable energy-harvesting devices," *Adv. Mater.*, vol. 30, no. 44, 2018, Art. no. 1801511.

[7] J. Kim, H. Kim, D. Kim, H.-J. Park, K. Ban, S. Ahn, and S.-M. Park, "A wireless power transfer based implantable ECG monitoring device," *Energies*, vol. 13, no. 4, p. 905, Feb. 2020.

[8] K. Agarwal, R. Jegadeesan, Y. Guo, and N. Thakor, "Wireless power transfer strategies for implantable bioelectronics," *IEEE Rev. Biomed. Eng.*, vol. 10, pp. 136–161, 2017.

[9] D. Kim, D. Jeong, J. Kim, H. Kim, J. Kim, S.-M. Park, and S. Ahn, "Design and implementation of a wireless charging-based cardiac monitoring system focused on temperature reduction and robust power transfer efficiency," *Energies*, vol. 13, no. 4, p. 1008, Feb. 2020.

[10] G. L. Barbruni, P. M. Ros, D. Demarchi, S. Carrara, and D. Ghezzi, "Miniaturised wireless power transfer systems for neurostimulation: A review," *IEEE Trans. Biomed. Circuits Syst.*, vol. 14, no. 6, pp. 1160–1178, Dec. 2020.

[11] A. Christ, M. Douglas, J. Nadakuduti, and N. Kuster, "Assessing human exposure to electromagnetic fields from wireless power transmission systems," *Proc. IEEE*, vol. 101, no. 6, pp. 1482–1493, Jun. 2013.

[12] R. Hinchet, H.-J. Yoon, H. Ryu, M.-K. Kim, E.-K. Choi, D.-S. Kim, and S.-W. Kim, "Transcutaneous ultrasound energy harvesting using capacitive triboelectric technology," *Science*, vol. 365, no. 6452, pp. 491–494, Aug. 2019.

[13] A. Kurs, A. Karalis, R. Moffatt, J. D. Joannopoulos, P. Fisher, and M. Soljačić, "Wireless power transfer via strongly coupled magnetic resonances," *Science*, vol. 317, no. 5834, pp. 83–86, 2007.

[14] J. S. Ho, S. Kim, and A. S. Y. Poon, "Midfield wireless powering for implantable systems," *Proc. IEEE*, vol. 101, no. 6, pp. 1369–1378, Jun. 2013.

[15] H. Basaeri, D. B. Christensen, and S. Roundy, "A review of acoustic power transfer for bio-medical implants," *Smart Mater. Struct.*, vol. 25, no. 12, Dec. 2016, Art. no. 123001.

[16] J.-D. Kim, C. Sun, and I.-S. Suh, "A proposal on wireless power transfer for medical implantable applications based on reviews," in *Proc. IEEE Wireless Power Transf. Conf.*, May 2014, pp. 166–169.

[17] M. G. L. Roes, J. L. Duarte, M. A. M. Hendrix, and E. A. Lomonova, "Acoustic energy transfer: A review," *IEEE Trans. Ind. Electron.*, vol. 60, no. 1, pp. 242–248, Jan. 2013.

[18] A. Denisov and E. Yeatman, "Ultrasonic vs. Inductive power delivery for miniature biomedical implants," in *Proc. Int. Conf. Body Sensor Netw.*, Jun. 2010, pp. 84–89.

[19] Int. Electrotechnical Commission, Switzerland, Standard ISO/IEC 60601-2-37, 2007.

[20] S. Q. Lee, W. Youm, and G. Hwang, "Biocompatible wireless power transferring based on ultrasonic resonance devices," in *Proc. Meetings Acoust. (ICA)*, vol. 19, no. 1, 2013, Art. no. 030030.

[21] Q. Shi, T. Wang, and C. Lee, "MEMS based broadband piezoelectric ultrasonic energy harvester (PUEH) for enabling self-powered implantable biomedical devices," *Sci. Rep.*, vol. 6, no. 1, pp. 1–10, Jul. 2016.

[22] R. O. Illing, J. E. Kennedy, F. Wu, G. R. T. Haar, A. S. Protheroe, P. J. Friend, F. V. Gleeson, D. W. Cranston, R. R. Phillips, and M. R. Middleton, "The safety and feasibility of extracorporeal high-intensity focused ultrasound (HIFU) for the treatment of liver and kidney tumours in a Western population," *Brit. J. Cancer*, vol. 93, no. 8, pp. 890–895, Oct. 2005.

[23] H. G. Lim, H. Kim, K. Kim, J. Park, Y. Kim, J. Yoo, D. Heo, J. Baik, S.-M. Park, and H. H. Kim, "Thermal ablation and high-resolution imaging using a back-to-back (BTB) dual-mode ultrasonic transducer: *in vivo* results," *Sensors*, vol. 21, no. 5, p. 1580, Feb. 2021.

[24] F. Duck and T. Leighton, "Frequency bands for ultrasound, suitable for the consideration of its health effects," *J. Acoust. Soc. Amer.*, vol. 144, no. 4, pp. 2490–2500, Oct. 2018.

[25] M. Gorostiaga, M. C. Wapler, and U. Wallrabe, "Optimizing piezoelectric receivers for acoustic power transfer applications," *Smart Mater. Struct.*, vol. 27, no. 7, Jul. 2018, Art. no. 075024.

[26] W. A. Smith, "Modeling 1-3 composite piezoelectrics: Hydrostatic response," *IEEE Trans. Ultrason., Ferroelectr., Freq. Control*, vol. 40, no. 1, pp. 41–49, Jan. 1993.

[27] R. E. Newnham, L. J. Bowen, K. A. Klicker, and L. E. Cross, "Composite piezoelectric transducers," *Mater. Des.*, vol. 2, pp. 93–106, Dec. 1980.

[28] W. A. Smith and B. A. Auld, "Modeling 1-3 composite piezoelectrics: Thickness-mode oscillations," *IEEE Trans. Ultrason., Ferroelectr., Freq. Control*, vol. 38, no. 1, pp. 40–47, Jan. 1991.

[29] R. Liu, K. A. Harasiewicz, and F. S. Foster, "Interdigital pair bonding for high frequency (20-50 MHz) ultrasonic composite transducers," *IEEE Trans. Ultrason., Ferroelectr., Freq. Control*, vol. 48, no. 1, pp. 299–306, Jan. 2001.

[30] B. Luo, X. Wang, Y. Wang, and L. Li, "Fabrication, characterization, properties and theoretical analysis of ceramic/PVDF composite flexible films with high dielectric constant and low dielectric loss," *J. Mater. Chem. A*, vol. 2, no. 2, pp. 510–519, 2014.

[31] S. Dash, R. N. P. Choudhary, and M. N. Goswami, "Enhanced dielectric and ferroelectric properties of PVDF-$BiFeO_3$ composites in 0–3 connectivity," *J. Alloys Compounds*, vol. 715, pp. 29–36, Aug. 2017.

[32] R. Liu, K. A. Harasiewicz, D. Knapik, N. A. Freeman, and F. S. Foster, "2–2 piezoelectric composites with high density and fine scale fabricated by interdigital pair bonding," *Appl. Phys. Lett.*, vol. 75, no. 21, pp. 3390–3392, Nov. 1999.

[33] C. Chang, K. Firouzi, K. K. Park, A. F. Sarioglu, A. Nikoozadeh, H.-S. Yoon, S. Vaithilingam, T. Carver, and B. T. Khuri-Yakub, "Acoustic lens for capacitive micromachined ultrasonic transducers," *J. Micromech. Microeng.*, vol. 24, no. 8, Aug. 2014, Art. no. 085007.

[34] P. Maréchal, F. Levassort, L.-P. Tran-Huu-Hue, and M. Lethiecq, "Lens-focused transducer modeling using an extended KLM model," *Ultrasonics*, vol. 46, no. 2, pp. 155–167, May 2007.

[35] H. J. Lee, S. Zhang, X. Geng, and T. R. Shrout, "Electroacoustic response of 1–3 piezocomposite transducers for high power applications," *Appl. Phys. Lett.*, vol. 101, no. 25, Dec. 2012, Art. no. 253504.

[36] S. Cho, J. Baik, R. Managuli, and C. Kim, "3D PHOVIS: 3D photoacoustic visualization studio," *Photoacoustics*, vol. 18, Jun. 2020, Art. no. 100168.

[37] N. Phipps, "Acoustic intensity measurement system: Application in localized drug delivery," M.S thesis, Dept. Elect. Eng., San Jose State Univ., San Jose, CA, USA, 2010.

[38] H. Vihvelin, J. Leadbetter, M. Bance, J. A. Brown, and R. B. A. Adamson, "Compensating for tissue changes in an ultrasonic power link for implanted medical devices," *IEEE Trans. Biomed. Circuits Syst.*, vol. 10, no. 2, pp. 404–411, Apr. 2016.

[39] K. Retz, S. Kotopoulis, T. Kiserud, K. Matre, G. E. Eide, and R. Sande, "Measured acoustic intensities for clinical diagnostic ultrasound transducers and correlation with thermal index," *Ultrasound Obstetrics Gynecol.*, vol. 50, no. 2, pp. 236–241, Aug. 2017.

[40] *Information for Manufacturers Seeking Marketing Clearance of Diagnostic Ultrasound Systems and Transducers Guidance for Industry and FDA Staff*, Food and Drug Administration, Silver Spring, MD, USA, 2008.

[41] L. Petrella, P. Fernandes, M. Santos, M. Caixinha, S. Nunes, C. Pinto, M. Morgado, J. Santos, F. Perdigão, and M. Gomes, "Safety assessment of an A-scan ultrasonic system for ophthalmic use," *J. Ultrasound Med.*, vol. 39, no. 11, pp. 2143–2150, Nov. 2020.

[42] T. A. Bigelow, C. C. Church, K. Sandstrom, J. G. Abbott, M. C. Ziskin, P. D. Edmonds, B. Herman, K. E. Thomenius, and T. J. Teo, "The thermal index: Its strengths, weaknesses, and proposed improvements," *J. Ultrasound Med.*, vol. 30, no. 5, pp. 714–734, May 2011.

[43] *Ultrasonics—Field Characterization—Test Methods for the Determination of Thermal and Mechanical Indices Related to Medical Diagnostic Ultrasonic Fields*, document IEC 62359, 2017.

[44] R. Bähring and C. K. Bauer, "Easy method to examine single nerve fiber excitability and conduction parameters using intact nonanesthetized earthworms," *Adv. Physiol. Educ.*, vol. 38, no. 3, pp. 253–264, Sep. 2014.

[45] M. Meng and M. Kiani, "Design and optimization of ultrasonic wireless power transmission links for millimeter-sized biomedical implants," *IEEE Trans. Biomed. Circuit Syst.*, vol. 11, no. 1, pp. 98–107, Feb. 2017.

[46] T. C. Chang, M. J. Weber, J. Charthad, S. Baltsavias, and A. Arbabian, "End-to-end design of efficient ultrasonic power links for scaling towards submillimeter implantable receivers," *IEEE Trans. Biomed. Circuits Syst.*, vol. 12, no. 5, pp. 1100–1111, Oct. 2018.

[47] D. Seo, J. Carmena, J. Rabaey, M. Maharbiz, and E. Alon, "Model validation of untethered, ultrasonic neural dust motes for cortical recording," *J. Neurosci. Methods*, vol. 244, pp. 114–122, Apr. 2015.

[48] S. H. Song, A. Kim, and B. Ziaie, "Omnidirectional ultrasonic powering for millimeter-scale implantable devices," *IEEE Trans. Biomed. Eng.*, vol. 62, no. 11, pp. 2717–2723, Nov. 2015.

[49] V. F.-G. Tseng, S. S. Bedair, and N. Lazarus, "Acoustic wireless power transfer with receiver array for enhanced performance," in *Proc. IEEE Wireless Power Transf. Conf. (WPTC)*, May 2017, pp. 1–4.

[50] V. F.-G. Tseng, S. S. Bedair, and N. Lazarus, "Phased array focusing for acoustic wireless power transfer," *IEEE Trans. Ultrason., Ferroelectr., Freq. Control*, vol. 65, no. 1, pp. 39–49, Jan. 2013.

[51] J. S. Han, C. W. Gal, J. M. Park, J. H. Kim, S. H. Lee, B. W. Yeo, B. W. Lee, S. S. Park, and S. J. Park, "Powder injection molding process for fabrication of piezoelectric 2D array ultrasound transducer," *Smart Mater. Struct.*, vol. 27, no. 7, Jul. 2018, Art. no. 075058.

[52] X.-J. Jiang, M.-W. Liu, F.-F. Shi, W. Wang, X.-M. Wu, and J.-Y. Chen, "A microscale linear phased-array ultrasonic transducer based on PZT ceramics," *Sensors*, vol. 19, no. 5, p. 1244, Mar. 2019.

[53] E. Mehdizadeh and G. Piazza, "AlN on SOI pMUTs for ultrasonic power transfer," in *Proc. IEEE Int. Ultrason. Symp. (IUS)*, Sep. 2017, pp. 1–4.

[54] H. Basaeri, Y. Yu, D. Young, and S. Roundy, "Acoustic power transfer for biomedical implants using piezoelectric receivers: Effects of misalignment and misorientation," *J. Micromech. Microeng.*, vol. 29, no. 8, Aug. 2019, Art. no. 084004.

[55] B. Herrera, F. Pop, C. Cassella, and M. Rinaldi, "AlN PMUT-based ultrasonic power transfer links for implantable electronics," in *Proc. 20th Int. Conf. Solid-State Sensors, Actuat. Microsyst. Eurosensors XXXIII (TRANSDUCERS EUROSENSORS XXXIII)*, Jun. 2019, pp. 861–864.

[56] C. Ju, E. Park, T. Kim, T. Kim, M. Kang, K.-S. Lee, and S.-M. Park, "Effectiveness of electrical stimulation on nerve regeneration after crush injury: Comparison between invasive and non-invasive stimulation," *PLoS ONE*, vol. 15, no. 5, May 2020, Art. no. e0233531.

[57] S. Sokolovic and S. Mehmedagic, "OS 11-06 the effect of vagus nerve stimulation on arterial hypertension using active implantable device," *J. Hypertension*, vol. 34, no. 1, p. e75, 2016.

[58] A. A. Bhide, V. Tailor, R. Fernando, V. Khullar, and G. A. Digesu, "Posterior tibial nerve stimulation for overactive bladder-techniques and efficacy," *Int. Urogynecol. J.*, vol. 31, no. 5, pp. 865–870, 2020.

[59] E. Park, J.-W. Lee, T. Kim, M. Kang, B. H. Cho, J. Lee, S.-M. Park, and K.-S. Lee, "The long-lasting post-stimulation inhibitory effects of bladder activity induced by posterior tibial nerve stimulation in unanesthetized rats," *Sci. Rep.*, vol. 10, no. 1, pp. 1–10, Dec. 2020.

KYUNGMIN KIM (Graduate Student Member, IEEE) received the B.S. degree in electronic engineering from Kyungpook National University, South Korea, in 2016. He is currently pursuing the M.S. and Ph.D. degrees with the Department of Convergence IT Engineering, POSTECH, South Korea. He has interested in piezoelectric material, MEMS, piezoelectric micromachined ultrasonic transducer (pMUT), device fabrication, and signal processing.

SEOK GEUN JANG received the B.S. degree in electronics engineering from Kyungpook National University, Daegu, South Korea, in 2019, and the M.S. degree in electrical engineering from the Pohang University of Science and Technology (POSTECH), Pohang, South Korea, in 2021.

HAE GYUN LIM received the B.S. degree in biochemistry from the University of California at Los Angeles, Los Angeles, CA, USA, in 2010, and the M.S. and Ph.D. degrees in biomedical engineering from the University of Southern California, Los Angeles, in 2014 and 2017, respectively. From 2013 to 2017, he was a Research Assistant with the NIH Resource Center for Medical Ultrasonic Transducer Technology. He worked as a Research Assistant Professor with the Future IT Innovation Laboratory, Pohang University of Science and Technology (POSTECH), Pohang, South Korea, in 2020. He is currently an Assistant Professor with the Department of Biomedical Engineering, Pukyong National University, Busan, South Korea. His research interests include ultrasonic transducers, cell mechanics, HIFU treatment, ultrasound imaging, and high frequency ultrasound microbeams.

HYUNG HAM KIM (Member, IEEE) received the B.S. degree in electrical engineering from the Korea Advanced Institute of Science and Technology, Daejeon, South Korea, in 1993, the M.S. degree in electrical engineering from Seoul National University, Seoul, South Korea, in 1995, and the M.S. and Ph.D. degrees in biomedical engineering from the University of Southern California, Los Angeles, CA, USA, in 2006 and 2010, respectively. He was the Manager and the Principal Engineer with the Department of Probe, Medison Company Ltd., Seoul, from 1994 to 2004, where he managed the research and development projects of medical ultrasound array transducers. He was a Research Assistant Professor with the Department of Biomedical Engineering, University of Southern California, where he was also the Manager of the NIH Resource Center for Medical Ultrasonic Transducer Technology. He joined Analogic Inc., Peabody, MA, USA, in 2014, where he led the research solutions business as the Director of business development, in 2016. He is currently an Associate Professor with the Department of Convergence IT Engineering, Department of Electrical Engineering, and the School of Interdisciplinary Bioscience and Bioengineering, Pohang University of Science and Technology (POSTECH), Pohang, South Korea. His current research interests include high frequency array transducers for high resolution ultrasound imaging, and cellular mechanics studies using high frequency ultrasound and neuromodulation using focused ultrasound.

SUNG-MIN PARK (Senior Member, IEEE) received the B.S. and Ph.D. degrees in electrical and computer engineering from Purdue University, West Lafayette, IN, USA, in 2001 and 2006, respectively. Since 2016, he has been with the Department of Convergence IT Engineering, Electrical Engineering, Mechanical Engineering, and the School of Interdisciplinary Bioscience and Bioengineering, Pohang University of Science and Technology (POSTECH), Pohang, South Korea, where he is currently a Professor. From 2006 to 2014, he was with Medtronic, Minneapolis, Minnesota, USA, as a Research and Development Manager, leading the award-wining effort in developing the world first MRI conditional pacemaker. From 2014 to 2016, he was with Samsung, Suwon, South Korea, as the Director, spearheading healthcare centric mobile device and mobile health service platform development projects.